Mon. Not. R. Astron. Soc. **318**, 67–72 (2000)

Sputtering in the outflows of cool stars

Carl Covatto★ and Per A. Aannestad
Dept. of Physics and Astronomy, Arizona State University, Tempe, AZ 85287-1504, USA

Accepted 2000 April 12. Received 2000 April 12; in original form 1999 October 21

ABSTRACT

Radiation pressure acts to accelerate dust grains and, by transfer of momentum through collisions with the gas, drives the outflows of late-type stars. Some of these dust–gas collisions may be energetic enough to remove atoms from the dust grains. From an assumed initial size distribution for the dust grains, the method of Krüger et al. is used to study the evolution of a sample of spherical amorphous carbon grains under conditions typical of a late-type star. The size distribution of dust grains is presented for various sets of model parameters. One set of models assumes an initial Mathis, Rumpl & Nordsieck (MRN) distribution for the dust grains. The high-luminosity (L_*), high-effective temperature ($T_{\rm eff}$) set of parameters has a terminal velocity ($v_{\rm term}$) that is near, but *above*, the upper limit of observed outflow velocities for carbon stars ($\sim$30 km s^{-1} for the assumed $\dot{M}$ of 5×10^{-6} M$_\odot$ yr^{-1}). The low L_*, $T_{\rm eff}$ model has a $v_{\rm term}$ that lies near, but *below*, the upper limit of observed velocities. A significant amount of sputtering occurs in the high L_*, $T_{\rm eff}$ model with $\sim$40 per cent of the grain mass sputtered. About $\sim$1 per cent of the dust mass is sputtered in the low L_*, $T_{\rm eff}$. Another set of models assumes that the dust forms with a log-normal distribution. Here, $v_{\rm term}$ is nearly the same for the high L_*, $T_{\rm eff}$ model as for the low L_*, $T_{\rm eff}$ model. This is a result of the large amount of dust mass loss ($\sim$75 per cent) by sputtering in the high L_*, $T_{\rm eff}$ model.

Key words: stars: AGB and post-AGB – circumstellar matter.

1 INTRODUCTION

It is widely believed that radiation pressure on dust is responsible for driving the outflows of late-type stars. Dust grains gain momentum by absorbing UV and optical photons. This momentum can then be transferred to the gas through collisions. The motions of the gas and dust are coupled.

To transfer momentum to the gas, the gas and dust must collide. Some of these collisions may be energetic enough to remove atoms from the surface of the dust. This is the process of physical sputtering. During the collision, the incident gas particle (the projectile) penetrates the surface of the dust grain (the target) and transfers momentum to the target atoms. For low-energy collisions (single knock-on regime), there are few collisions with enough energy to displace target atoms from their locations with enough energy to escape from the surface of the target (Sigmund 1981). The escaping atoms determine the sputtering yield (emitted atoms/incident particle).

There are two types of physical sputtering: thermal and non-thermal. Thermal sputtering takes place among gas particles, the thermal energy of which is high enough to cause the removal of atoms from the target surface. Non-thermal sputtering occurs among particles the translational kinetic energy of which is large enough to remove atoms from the target surface. The thermal sputtering yield is proportional to the Boltzmann factor. At the low temperatures found in carbon star atmospheres, the thermal sputtering yield will be small compared to the non-thermal sputtering yield. We therefore ignore thermal sputtering. Hereafter, we use the term sputtering to mean non-thermal sputtering.

There have been many recent papers studying grain growth and the dynamics of stellar outflows (Krüger & Sedlmayr 1997; Steffen et al. 1997; Ivezić & Elitzur 1995; Habing, Tignon & Tielens 1994; Dominik, Gail & Sedlmayr 1989). Excellent reviews of these subjects may be found in Sedlmayr & Dominik (1995) and the proceedings edited by De Greve, Blomme & Hensberge (1997).

The purpose of this work is the construction of a simple dynamical model that can be used to find the changes in the size distribution of dust grains arising from destructive processes in the outflows of late-type stars.

The paper is structured as follows: Section 2 describes the model, Section 3 describes the model values and initial conditions, Section 4 describes the results, and the conclusions are given in Section 5.

2 MODEL

A general method, assuming spherical symmetry, of following the evolution of a dust size distribution undergoing either growth and/or destruction was developed by Krüger, Woitke & Sedlmayr

★ E-mail: carl.covatto@asu.edu (cc)

(1995, hereafter KWS). This method can be used to process an assumed grain size distribution. KWS separates destruction mechanisms into two types: continuous and discontinuous. A continuous process is defined as one that smoothly changes grain sizes, such as sputtering. Discontinuous processes are those that abruptly change the grain size, such as shattering in a grain–grain collision.

If dust nucleation and discontinuous processes are neglected, the equation that determines the grain size distribution is

$$-r_0^2 v_{\rm d}(a_0, r_0) f(a_0, r_0) + r^2 \frac{{\rm d}a}{{\rm d}a_0} v_{\rm d}(a, r) f(a, r) = 0, \tag{1}$$

where r_0 and r are the initial and current radial positions, $v_{\rm d}(a_0, r_0)$ and $v_{\rm d}(a, r)$ are the initial and current velocities of the dust grains, $f(a_0, r_0)$ and $f(a, r)$ are the initial and current grain size distributions, and ${\rm d}a/{\rm d}a_0$ is the derivative of the current grain size (a) with respect to the initial grain size (a_0). This is equation 15 in KWS with slightly different notation. We set $\zeta = a_0$ (instead of $a*$) and $a_r = a$, the second term on the left-hand side is set equal to zero (no nucleation), and the right-hand side is also set equal to zero (no source term). If we solve equation (1) for the current grain size distribution, we get

$$f(a, r) = \frac{v_{\rm d}(a_0, r_0)}{v_{\rm d}(a, r)} \frac{r_0^2}{r^2} \frac{f(a_0, r_0)}{\dfrac{{\rm d}a}{{\rm d}a_0}}. \tag{2}$$

When the grains do not change size, ${\rm d}a/{\rm d}a_0 = 1$ and equation (2) then becomes $fvr^2 = \text{constant}$. The grain size distribution will only be modified by a combination of geometrical and dynamical dilution effects. The value of the derivative in equation (2) is found using the analytic derivative of the Lagrange interpolating polynomial. For more details see KWS, Section 3.2.

To calculate the grain size distribution, we must know the velocity of the dust grains. In this work, the motion of the gas and dust will be found from their respective differential equations. The motion of the $i^{\rm th}$ dust grain can be described by

$$v_{\rm d}(a_i) \frac{{\rm d}v_{\rm d}(a_i)}{{\rm d}r} = \frac{3L_* Q_{\rm pr}(a_i)}{16\pi\rho_{\rm s} a_i c r^2} - \frac{GM_*}{r^2} - \frac{3\dot{M}}{16\pi\rho_{\rm s} a_i r^2 v_{\rm g}} 2c_{\rm T}^2 F(s_i), \tag{3}$$

where L_* is the luminosity of the central star, $Q_{\rm pr}$ is the flux-averaged pressure coefficient, ρ_s is the bulk density of the dust material, M_* is the mass of the central star, $\dot{M}$ is the mass loss rate, $v_{\rm g}$ is the gas velocity (see below), and $c_{\rm T}$ is the isothermal sound speed. The function $F(s_i)$ is given by

$$F(s_i) = [1 + s_i^2 - (0.17 s_i^2 + 0.5|s_i| + 1)^{-3}]{\rm sgn}(s_i), \tag{4}$$

where $s_i = \sqrt{\frac{1}{2}}[v_{\rm d}(a_i) - v_{\rm g}]/c_{\rm T}$.

The first term in equation (3) represents the acceleration of the grains as a result of radiation pressure, the second term is the acceleration arising from gravity, and the third term is the acceleration arising from collisions with the gas. This form of the collisional drag force (third term) is an analytic fit by Berruyer & Frisch (1983) to the model of Baines, Williams & Asebiomo (1965), which describes the drag force felt by a sphere moving through a gas in the specular reflection limit. The specular reflection limit assumes that the normal velocity components reverse direction upon impact.

The grains are assumed to be spherical and made of amorphous carbon. The pressure coefficients are calculated from Mie theory (Bohren & Huffman 1983) and then averaged over a blackbody spectrum with effective temperature $T_{\rm eff}$. The optical constants used are from Rouleau & Martin (1991) material AC1.

The equation of motion for the gas is

$$v_{\rm g} \frac{{\rm d}v_{\rm g}}{{\rm d}r} = -\frac{1}{\rho}\frac{{\rm d}P}{{\rm d}r} - \frac{GM_*}{r^2} + 2c_{\rm T}^2 \int_{a_{\rm min}}^{a_{\rm max}} \pi a^2 f(a) F(s)\, {\rm d}a, \tag{5}$$

where we use the trapezoid rule to evaluate the integral over the complete range of the size distribution. The first term on the right-hand side of equation (5) is the pressure gradient, the second term is the gravitational acceleration, and the third term is the total acceleration received by the gas through collisions with the dust. If we describe the gas pressure by $P = c_{\rm T}^2 \rho$, the above equation can be written in the form of a wind equation:

$$\frac{1}{v_{\rm g}} \frac{{\rm d}v_{\rm g}}{{\rm d}r} = \frac{\dfrac{2c_{\rm T}^2}{r} - \dfrac{c_{\rm T}^2}{T}\dfrac{{\rm d}T}{{\rm d}r} - \dfrac{GM_*}{r^2} + 2c_{\rm T}^2 \displaystyle\int \pi a^2 f(a) F(s)\, {\rm d}a}{v_{\rm g}^2 - c_{\rm T}^2}, \tag{6}$$

where the isothermal sound speed is

$$c_{\rm T} = \sqrt{\frac{kT}{\mu m_{\rm H}}},$$

with μ being the mean molecular weight of the gas. Again, the integral in equation (6) is evaluated over the whole range of the size distribution using the trapezoid rule.

The grain sizes also need to be computed. This can be done from (Dominik et al. 1989):

$$\frac{{\rm d}a}{{\rm d}r} = \frac{1}{v_{\rm d}(a, r)} \frac{1}{\tau_{\rm net}(a, r)} \frac{\xi}{d}, \tag{7}$$

where $\tau_{\rm net}^{-1}(a, r)$ is the net growth rate (s^{-1}; see below), ξ is the hypothetical radius of a monomer and is given by

$$\left(\frac{3Am_{\rm H}}{4\pi\rho_{\rm s}}\right)^{\frac{1}{3}}$$

with $Am_{\rm H}$ being the mass of the sputtered atoms, and d is the fractal dimension of the dust grain ($d = 3$ for spheres).

The sputtering rates are computed using the theory as summarized in Tielens et al. (1994). The (negative) growth rate may be written as $\tau_{\rm net}^{-1} = -\pi\xi^2 (v_{\rm d} - v_{\rm g}) n_{\rm H} \Sigma_i A_i Y_i$, where $n_{\rm H}$ is the number density of hydrogen, A_i is the abundance by number of the $i^{\rm th}$ gas element relative to hydrogen, and Y_i is the sputtering yield for normal incidence given by equation (4.13) of Tielens et al. (1994). The sum is performed over the total number of different gas species. The grains are assumed to be electrically neutral. The number density of hydrogen is found from the gas density which is related to the mass-loss rate through the continuity equation $\dot{M} = 4\pi r^2 \rho v_{\rm g}$ with $\rho = \mu m_{\rm H} n_{\rm H}$. The angle-averaged sputtering yield

$$\bar{Y} = 2\int_0^{\frac{\pi}{2}} Y_i(\theta) \cos\theta \sin\theta\, {\rm d}\theta \approx 2Y_i(\theta = 0)$$

assumes a $(\cos\theta)^{-1}$ for $Y_i(\theta)$ (Draine 1996). Recent Monte Carlo simulations by Jurac, Johnson & Donn (1998) show that the yield can differ significantly from a $(\cos\theta)^{-1}$ dependence and so we choose to use the normal incidence yield and set $Y_i = Y_i(\theta = 0)$.

Equations 3, 6, and 7 give a system of $2n+1$ coupled, first-order differential equations where n is the total number of grain sizes. This system can be integrated outward using a fourth-order Runge–Kutta method with an adaptive step-size control (Press et al. 1992).

3 MODEL VALUES AND INITIAL CONDITIONS

We must pick values of M_*, L_*, T_*, and the elemental abundances. Unlike the work of Krüger & Sedlmayr (1997), we do not force the numerator of equation (6) to be zero at the sonic point where $v_g = c_T$, and so the value of $\dot{M}$ does not follow as an eigenvalue of the solution and must be specified. The temperature structure must also be specified. We take $\rho_s = 1.85\,\mathrm{g\,cm^{-3}}$ and $\mu = 1.4$.

We assume the dust initially is distributed either by an MRN distribution (as given in Mathis, Rumpl & Nordsieck 1977) or by a log-normal distribution. The MRN distribution is defined as

$$f(a)da = A_k n_H a^{-3.5}\,da \tag{8}$$

where A_k is the normalization and the log-normal distribution is given by

$$f(a)da = \frac{A_k n_H}{\sqrt{\pi}\ln\sigma}\frac{1}{a}\exp\left[-\left(\frac{\ln\left(\frac{a}{\bar{a}}\right)}{\sqrt{2}\ln\sigma}\right)^2\right]da \tag{9}$$

where $\bar{a}$ is related to the average size of the distribution and σ is related to its width. We choose the MRN distribution because of its pervasiveness in the literature. However, for a size distribution that is evolving by random particle collisions (coagulation), Castleman (1979) suggests that the log-normal distribution seems to fit numerical solutions of the Smoluchowski equation. The log-normal distribution resembles the calculated distributions of Dominik et al. (1989) and Krüger & Sedlmayr (1997). The size range of the MRN distribution was chosen to be $a_{min} = 0.001\,\mu m$ to $a_{max} = 0.25\,\mu m$ and for the log-normal distribution we choose $a_{min} = 0.001\,\mu m$ to $a_{max} = 0.50\,\mu m$. Also, for the log-normal distribution, we take $\bar{a} = 0.1\,\mu m$ and $\sigma = 1.4$. The dust size distributions are normalized so that the dust-to-gas mass ratio is 0.0015.

To minimize the errors when evaluating the integral in equation (6), a large number of grain sizes are necessary. However, a price must be paid in that more grains means more computing time. We choose 40 grain sizes which seems to be a good compromise between accumulated errors and total computation time. Because we know the smaller grains are more closely coupled to the gas, none of the smallest grain sizes will be affected by sputtering. This means that the total number of grains is conserved and we will use this as an indication of the accuracy of the numerical integration.

Table 1 shows the velocity and energy thresholds for sputtering. The threshold energy is related to the surface binding energy (U_0) and has a value near 7 eV for amorphous carbon (Kelires 1992). However, a value near 4 eV better matches measured sputtering yields (Eckstein, Sagara & Kamada 1987; Tielens et al. 1994). As the amorphous carbon grains are accelerated in the outflow, they will collide with hydrogen atoms. These collisions will not be energetic enough to sputter carbon atoms from the grain surface. However, the surface of the grain will be chemically altered. The resulting compounds generally have a lower surface binding energy than the unaltered grain material (Hsu 1988; Roth 1983). The reduced binding energy may be low enough so that the new compounds may be able to desorb from the grain surface depending on the grain temperature. This is known as chemical sputtering and will be the subject of future work.

The abundances by number relative to H for H, He, C, N, and O are also shown in Table 1. The C and N abundances are taken as solar and C/O = 1.3. Fig. 1 shows $A_i Y_i$ plotted versus the velocity of the impact. Sputtering by C and O is important at velocities less than $\sim$35 km s^{-1} where sputtering by He begins to dominate. As a result of its low abundance, N plays little or no role here. Monte Carlo simulations by Field et al. (1997) have found that significant sputtering occurs at energies higher than previously thought. Their sputtering yields are about two orders of magnitude lower than the yields used in this work. However, note that they use 7.41 eV for their surface binding energy as opposed to the 4 eV used here.

Table 1. Sputtering thresholds.

Element	A_i	v_{thresh}(km s^{-1})	E_{thresh}(eV)
H	1	61.4	19.7
He	0.1	32.6	22.2
C	4.7×10^{-4}	22.6	32.0
N	9.8×10^{-5}	21.5	33.7
O	3.6×10^{-4}	20.6	35.2

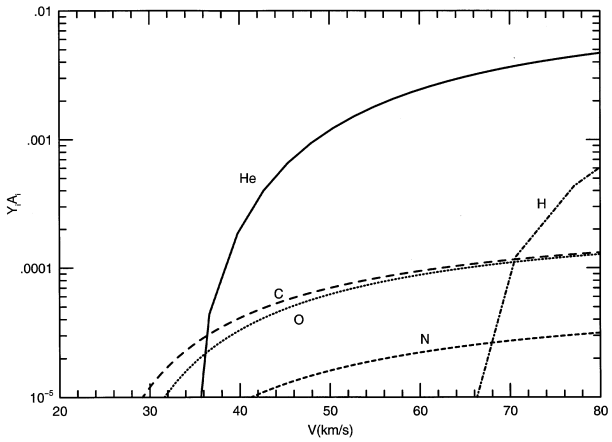

Figure 1. The sputtering yields for H, He, C, N and O impacting an amorphous carbon target as a function of the collisional velocity. The yield is multiplied by the abundance by number relative to hydrogen.

To avoid the singularity in equation (6), the calculation is started at $r = r_0$, just beyond the sonic point at which the dust and gas are assumed to have initial velocities that are slightly larger than c_T. All of the dust is assumed to form at the point at which the gas temperature drops below the condensation temperature, which is taken to be 1000 K. We assume a power-law temperature structure

$$T(r) = T_{eff}\left(\frac{R_*}{r}\right)^n$$

(Gail & Sedlmayr 1985), where the size of the star (R_*) is determined from $L_* = 4\pi R_*^2 \sigma T_{eff}^4$. All calculations are stopped at 1.0×10^{17} cm, which is sufficiently far from the starting point that the velocities and grain sizes change very little between successive steps.

4 RESULTS AND DISCUSSION

A series of models were calculated for different model parameters and initial dust distributions. The model parameters are given in Table 2 and are labelled by the letters a–d. The resulting outflow velocities are listed in Table 3 and are labelled by an integer (1 or 2) which denotes the assumed dust distribution followed by a

Table 2. Model parameters.

Model Number	$M*(M_\odot)$	$L*(L_\odot)$	$T_{\rm eff}$ (K)	$\dot{M}(M_\odot\,{\rm yr}^{-1})$	n	$R*$(cm)	r_0(cm)
T	1	1.0×10^4	2000	3.0×10^{-6}	0.6	5.92×10^{13}	1.88×10^{14}
a	1	7.3×10^4	2500	5.0×10^{-6}	0.6	1.02×10^{14}	4.72×10^{14}
b	1	7.3×10^4	2500	5.0×10^{-6}	0.7	1.02×10^{14}	3.79×10^{14}
c	1	1.1×10^4	2000	5.0×10^{-6}	0.6	6.21×10^{13}	1.97×10^{14}
d	1	1.1×10^4	2000	5.0×10^{-6}	0.7	6.21×10^{13}	1.67×10^{14}

Table 3. Model values.

Model number	Dust distribution	$v_{\rm term}({\rm km\,s^{-1}})$	$\frac{\chi}{\chi_i}$
T	MRN	23.1	1.00
1a	MRN	34.2	0.609
1b	MRN	37.4	0.587
1c	MRN	25.2	0.995
1d	MRN	27.1	0.993
2a	LN	28.0	0.271
2b	LN	29.6	0.237
2c	LN	27.3	0.991
2d	LN	29.6	0.987

letter (a–d) which indicates which set of model parameters was used.

A test calculation with model parameters T assuming an MRN distribution for the dust was run without any sputtering ($\tau_{\rm net}^{-1}=0$). The terminal velocities of the dust grains were checked against the values predicted by setting the right-hand side of equation (3) equal to zero, neglecting the gravitational term, and then solving the resulting polynomial equation for $v_{\rm d}(a_i)$. The computed results differed from the derived results by $\leqslant$0.1 per cent. The resulting outflow velocity was $23.1\,{\rm km\,s^{-1}}$.

By ignoring radiative transfer effects, this model for a radiation-pressure driven stellar outflow is limited to the optically thin case (low mass-loss rates). We therefore pick extremes in luminosity to study the effect of sputtering on the dust size distribution. We also vary the power-law index for the gas temperature, where we have $n=0.6$ for the a models and $n=0.7$ for the b models.

The models labelled by 1a–1d were calculated assuming the dust formed with an MRN distribution. We chose the 40 grain sizes to be equally spaced logarithmically. Here the number density ratio was conserved to better than 1 per cent. Fig. 2 shows the resulting gas outflow velocity as a function of radial position. As can be expected, the higher luminosity models give larger outflow velocities. Also, the models with a temperature power-law index of $n=0.7$ have a higher outflow velocity than the models with $n=0.6$. This can be seen from the second term of equation (6). The temperature gradient is larger in the models with $n=0.7$ and will produce a larger gas velocity.

The catalogue of CO and HCN observations by Loup et al. (1993) show the distribution of expansion velocities ($v_{\rm term}$) for C-rich sources to peak at 10–15 $\rm km\,s^{-1}$. The full range of observed velocities is from 5 to 35 $\rm km\,s^{-1}$. Their fig. 8 shows the mass-loss rate derived from CO observations plotted versus $v_{\rm term}$ and shows a spread at any given $\dot{M}$. At $\dot{M}=5\times10^{-6}\,M_\odot\,{\rm yr}^{-1}$, the range of $v_{\rm term}$ is 10 to 30 $\rm km\,s^{-1}$. The sample of Zuckerman & Dyck (1989) also shows a spread in $v_{\rm term}$ of 5 to 35 $\rm km\,s^{-1}$ for galactic carbon stars. They find that the stars that have $v_{\rm term}\geqslant 18\,{\rm km\,s^{-1}}$ lie near the galactic plane ($|b|\leqslant10°$).

Zuckerman & Dyck suggest that some of the observed spread in $v_{\rm term}$ is a result of differences in luminosity. With all other parameters being equal, a larger luminosity will produce a higher

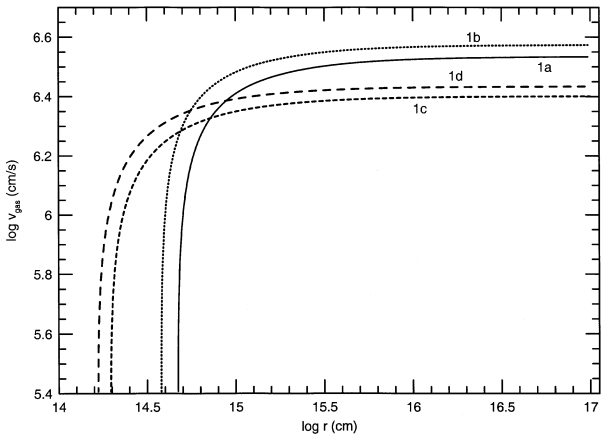

Figure 2. Gas velocity versus r for models 1a–1d. Models 1a and 1b have $L*$, $T_{\rm eff}$ larger than models 1c and 1d which results in a higher terminal velocity. Models 1a and 1b also undergo more sputtering. The models with a higher temperature power-law index ($n=0.7$; models 1b and 1d) have a higher terminal velocity than the models with a lower temperature power-law index ($n=0.6$; models 1a and 1c).

$v_{\rm term}$ (however, see the discussion below). This can be seen from equation (3). They also claim that metallicity differences may play a role because a star with a lower metallicity will have a lower dust-to-gas mass ratio. Using the parameters of the model T with an MRN distribution, but decreasing the dust-to-gas mass ratio to 0.001, produced an outflow velocity of $17.7\,{\rm km\,s^{-1}}$.

In the present work, for the assumed $\dot{M}$, $v_{\rm term}$ for models 1a and 1b lie above the largest observed values and $v_{\rm term}$ for models 1c and 1d lie below the upper limits of observed values. The high outflow velocity for models 1a and 1b is a result of the unusually large value of luminosity combined with the low mass-loss rate. The mass-loss rate is related to the gas density via the continuity equation. The low mass-loss rate means that there is less gas present to help decelerate the dust grains.

The undiluted size distribution of the dust grains for model 1a at four locations is shown in Fig. 3. The unbent line represents the initial size distribution at the start of the calculation ($r=r_0$). It is a straight line with a slope of -3.5. At $1.4r_0$, the size distribution for sizes below $\sim$0.07 μm remains unchanged. The grains that were previously larger than 0.07 mu;m have 'piled up' here. The situation is similar at $42r_0$ and at $212r_0$. The effects of geometrical and dynamical dilution have been removed to better show the variations in the size distribution arising from sputtering. A similar result is obtained for the undiluted size distribution of model 1b.

The ratio of the final to initial dust-to-gas mass ratio can be computed from

$$\frac{\chi_{\rm f}}{\chi_{\rm i}}=\frac{\rho_{\rm d,f}}{\rho_{\rm d,i}}\frac{\rho_{\rm g,i}}{\rho_{\rm g,f}}=\frac{\int a^3 f(a,r)\,{\rm d}a}{\int a_0^3 f(a_0,r_0)\,{\rm d}a_0}\left(\frac{\rho_{\rm g,i}}{\rho_{\rm g,f}}\right). \qquad (10)$$

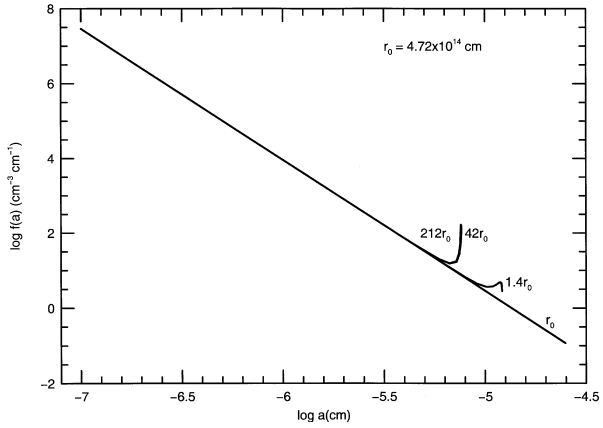

Figure 3. The grain size distribution at various radial positions for model 1a. By $r = 1.4r_0$ the distribution has been modified from its initial power-law form for $a > 0.04\,\mu$m. Beyond $r = 43r_0$ very little sputtering takes place because of the decrease in gas density. When the calculation is stopped, the largest unchanged grain size is $\sim$0.03 μm and the largest grain size is $\sim$0.076 μm.

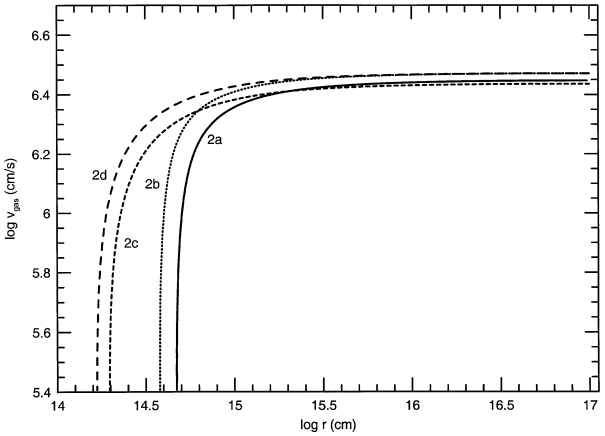

Figure 4. Gas velocity versus r for models 2a–2d. All models, regardless of the stellar parameters, have nearly the same terminal velocity. The dust in models 2a and 2b is heavily sputtered. Although models 2a and 2b have a higher luminosity than models 2c and 2d there is little dust remaining to drive the outflow and so a lower terminal velocity is reached.

If we drop the dilution factors from the ratio of the gas densities ($\rho v_g r^2 =$ constant) and assume that the gas mass does not change very much from the addition of sputtered atoms, then $\rho_{g,i} \approx \rho_{g,f}$. This is a safe assumption. If all of the dust were returned to the gas phase, the mass would be changed by about 0.1 per cent. From equation (2) we can see that the size distribution of dust is diluted by dynamical and geometrical factors relative to its initial value. Because we want to directly compare the amount of dust mass present, we must 'undilute' $f(a, r)$ before integrating over the current range of a. In the numerator of equation (8), we replace $f(a)$ by $f(a_0, r_0)(\mathrm{d}a/\mathrm{d}a_0)^{-1}$. For model 1a, this ratio is 0.609. About 40 per cent of the dust mass is sputtered away. In model 1b this ratio is 0.587. The higher terminal velocity model produced more sputtering. The maximum surviving grain size for model 1a is 0.076 μm.

The undiluted size distributions for model 1c and 1d (not shown) look like straight lines of slope -3.5 on a log–log scale. Very little sputtering occurs in these calculations. By the time the grains build up enough velocity relative to the gas, the gas density has dropped enough so that the sputtering rate is very small.

The models labelled 2a–2d use the same model parameters as the above models, but assume that the dust initially has a log-normal distribution. As a result of the extended size range and because the peak of the initial distribution is smaller than the final maximum grain size, we had to redistribute the initial grain sizes so that the number density ratio is constant to better than 1 per cent. The grain sizes were chosen so that they are more closely spaced at the large end of the size range.

Fig. 4 shows the outflow velocities for models 2a–2d as a function of radial position. All models have a velocity near the upper limit of the observed outflow velocities from the Loup (1993) and the Zuckerman & Dyck (1989) samples. Here, our intuition seems to fail. The models with the higher luminosity (2a and 2b) do not necessarily give the highest outflow velocity. Much of the dust mass is sputtered away ($\sim$75 per cent) and so there is little dust left to drive the outflow. If we shift the position of the peak of the initial size distribution by changing $\bar{a}$ from 0.1 μm to 0.01 μm, we find the outflow velocity increases to 42.4 km s^{-1} and the change in dust mass arising from sputtering is less than 1 per cent. This happens despite the fact that the maximum surviving grain size is 0.070 μm as opposed to 0.081 μm for the case in which $\bar{a} = 0.1\,\mu$m.

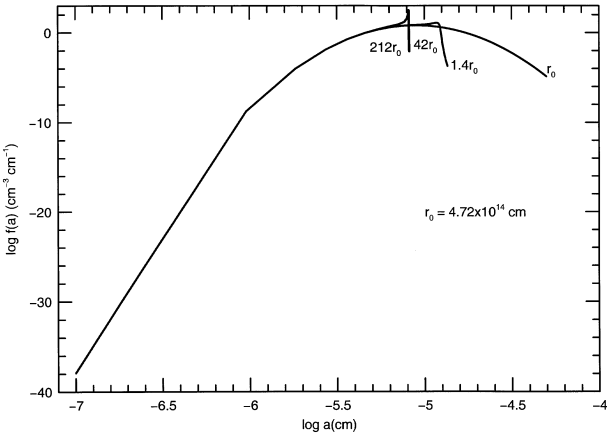

Figure 5. The grain size distribution for model 2a at different radial positions. By $r = 1.4r_0$ the distribution has been modified from its initial log-normal form for $a > 0.04\,\mu$m. Beyond $r = 43r_0$ little sputtering takes place because of the decrease in gas density. When the calculation is stopped the largest unchanged grain size is $\sim$0.03 μm and the largest grain size is 0.081 μm. The kink in the curve at $\log a = -6$ is a result of the large distance between the dust sizes in this region of the distribution.

Even though the two assumed initial dust distributions are very different from each other, we see that the maximum surviving grain size is nearly the same for models 1a and 2a. This suggests that the largest surviving grain size depends on the model parameters and not on the choice of the initial dust size distribution.

The undiluted dust distribution for model 2a is shown in Fig. 5. The curve labelled with r_0 is the initial dust size distribution. There are similarities to Fig. 3. The large size end of the dust distribution is sputtered away by $r = 1.4r_0$. We also see that very little sputtering takes place beyond $r = 42r_0$. Note the kink in the curve at $\log a = -6$ is from a lack of dust sizes in that region; they were more strongly concentrated in the region where sputtering would take place. A similar result (not shown) for model 2b is obtained.

The undiluted dust distribution for models 2c and 2d are not shown, but closely resemble the initial log-normal distribution. This is because of the minimal amount of sputtering which takes place.

As with models 1, models 2 also show a higher outflow velocity for the cases where $n = 0.7$ as opposed to $n = 0.6$. The location where the dust is 'created' is found to have an effect on the end results. Comparing the models with $n = 0.6$ to those with $n = 0.7$, we see that the $n = 0.7$ models have higher outflow velocities than the $n = 0.6$ models and thus the dust undergoes more sputtering. It is important, then, to get the gas temperature structure correct. A simple power law will suffice at low mass-loss rates ($\leqslant 10^{-6}\,\mathrm{M}_{\odot}\,\mathrm{yr}^{-1}$) where the dust shell is optically thin (Krüger 1997, figure 4.2). However, at high mass-loss rates where the dust shell is optically thick, a simple power law does not accurately describe the whole dust shell (Krüger 1997, figure 4.10).

5 CONCLUSIONS

A simple dynamical model was developed so that changes in a dust size distribution could be followed. All the models except 1a and 1b have v_{term} near or just below the maximum observed outflow velocities of carbon stars for $\dot{M} = 5.0 \times 10^{-6}\,\mathrm{M}_{\odot}\,\mathrm{yr}^{-1}$. In models 1a and 1b, the dust-to-gas mass ratio changed by nearly 40 per cent because of sputtering, and in models 2a and 2b it changed by about 75 per cent. As the larger grains decrease in size, they begin to pile up at the size below which no sputtering can occur, causing the size distribution to deviate from its initial shape. The dust-to-gas mass ratio for models 1c, 1d, 2c, and 2d changed by $\sim$1 per cent and little difference can be seen in the size distribution of dust grains.

In order to investigate models with higher mass-loss rates, the temperature structure must be determined accurately. For example, one could use the grey atmosphere approximation (Mihalas 1970; Krüger 1997). Also, computing the optical depth through the dust shell may be important in modifying the radiation field. This will change the average value of Q_{pr} and thus change the momentum gained by the dust.

ACKNOWLEDGMENTS

The authors would like to thank Rogier Windhorst for providing computing facilities. This work was funded in part by a NASA Space Grant.

REFERENCES

Baines M. J., Williams I. P., Asebiomo A. S., 1965, MNRAS, 130, 63
Berruyer N., Frish H., 1983, A&A, 126, 269
Bohren C. F., Huffman D. R., 1983, Absorption and Scattering of Light by Small Particles. Wiley, New York
Castleman A. W., 1979, Ap&SS, 65, 337
De Greve J. P., Blomme R., Hensberge H., eds, 1997, Stellar Atmospheres: Theory and Observation. Springer-Verlag, Berlin
Dominik C., Gail H.-P., Sedlmayr E., 1989, A&A, 223, 236
Draine B. T., 1996, in Millar T. J., ed., Shocks in Astrophysics. Kluwer, Dordrecht
Eckstein W., Sagara A., Kamada K., 1987, J. Nucl. Mat., 150, 266
Field D., May P. W., Pineau des Forêts G., Flower D. R., 1997, MNRAS, 285, 839
Gail H.-P., Sedlmayr E., 1985, A&A, 148, 183
Habing H. J., Tignon J., Tielens A. G. G. M., 1994, A&A, 286, 523
Hsu W. L., 1988, J. Vac. Sci. Tech. A, 6, 1803
Ivezić Ž., Elitzur N., 1995, ApJ, 445, 415
Jurac S., Johnson R. E., Donn B., 1998, ApJ, 503, 247
Kelires P. C., 1992, Phys. Rev. Lett., 68, 1854
Krüger D., 1997, PhD thesis, Technische Universität Berlin
Krüger D., Sedlmayr E., 1997, A&A, 321, 557
Krüger D., Woitke P., Sedlmayr E., 1995, A&AS, 113, 593 (KWS)
Loup C., Forveille T., Omont A., Paul J. F., 1993, A&AS, 99, 291
Mathis J. S., Rumpl W., Nordsieck K. H., 1977, ApJ, 217, 425 (MRN)
Mihalas D., 1970, Stellar Atmospheres. Freeman, San Francisco
Press W. H., Teukolsky S. A., Vetterling W. T., Flannery B. P., 1992, Numerical Recipes in FORTRAN, 2nd edn. Cambridge Univ. Press, Cambridge
Roth J., 1983, in Behrisch R., ed., Sputtering by Particle Bombardment II. Springer-Verlag, Berlin
Rouleau F., Martin P. G., 1991, ApJ, 377, 526
Sedlmayr E., Dominik C., 1995, Space Sci. Rev., 73, 211
Sigmund P., 1981, in Behrisch R., ed., Sputtering by Particle Bombardment I. Springer-Verlag, Berlin
Steffen M., Szczerba R., Men'shchikov A., Schönberner D., 1997, A&AS, 126, 39
Tielens A. G. G. M., Mckee C., Seab C. B., Hollenbach D. J., 1994, ApJ, 431, 321
Zuckerman B., Dyck H. M., 1989, A&A, 209, 119

This paper has been typeset from a TEX/LATEX file prepared by the author.